Available online at www.sciencedirect.com
SCIENCE DIRECT®
International Journal of Non-Linear Mechanics 40 (2005) 165–175
INTERNATIONAL JOURNAL OF NON-LINEAR MECHANICS
www.elsevier.com/locate/nlm

Elastic instabilities in rubber☆

A.N. Gent

The University of Akron, Akron, OH 44325-3909, USA

Received 20 May 2004; accepted 20 May 2004

Abstract

Materials that undergo large elastic deformations can exhibit novel instabilities. Several examples are considered here: development of an aneurysm on inflating a cylindrical rubber tube; non-uniform stretching on inflating a spherical balloon; expansion of small cavities in rubber blocks when they are subjected to a critical amount of triaxial tension or when they are supersaturated with a dissolved gas; wrinkling of the surface of a block at a critical amount of compression; and the sudden formation of "knots" on twisting stretched cylindrical rods. These various deformations are analyzed in terms of simple strain energy functions using Rivlin's theory of large elastic deformations. The theoretical results are then compared with experimental measurements of the onset of unstable states. Such comparisons provide new tests of Rivlin's theory and, at least in principle, critical tests of proposed strain energy functions for rubber. Moreover, the onset of highly non-uniform deformations has serious implications for the fatigue life and fracture resistance of rubber components.

Keywords: Elasticity; Instabilities; Rubber

1. Introduction

When rubber is subjected to certain simple deformations an unstable condition is reached at a critical point. Part of the sample suddenly becomes highly deformed while the remainder appears largely unchanged, its deformation actually becoming somewhat smaller. A review is given here of several examples of the onset of non-uniform deformations as a result of an inherent elastic instability. In each case experimental observations of the critical condition are compared with the predictions of Rivlin's theory of large elastic deformations [1,2], making use of simple strain energy functions. This comparison is important for two reasons: it provides a critical test of the theoretical analysis and its applicability to real materials, and it also tests the validity of proposed strain energy functions in a new way. There are also serious implications for the fracture and fatigue life of rubber components when highly non-uniform deformations occur.

We first discuss the known elastic behavior of rubber in terms of the strain energy function W that relates the amount of elastic energy to the amount of strain imposed, and then the stress–strain relations that follow from a given function W. Several examples of unstable deformations are then considered, both theoretically and experimentally.

2. Elastic behavior of rubber

2.1. Strain energy functions

A few simple strain energy functions are employed here. They are relations between the strain energy

☆ Dedicated to Niall Horgan on the occasion of his 60th birthday.

E-mail address: gent@uakron.edu (A.N. Gent).

0020-7462/$ - see front matter © 2004 Elsevier Ltd. All rights reserved.
doi:10.1016/j.ijnonlinmec.2004.05.006

density W per unit volume and the imposed deformation. They are all based on assumptions of incompressibility in bulk, isotropy in the undeformed state, and reversible stress–strain relations, i.e. perfect elasticity.

The first relation for W, termed neo-Hookean by Rivlin because of its simplicity, is

$$W = (G/2)J_1, \tag{1}$$

where G is an elastic coefficient (equal to the shear modulus at small strains) and J_1 is a scalar measure of strain, given by

$$J_1 = \lambda_1^2 + \lambda_2^2 + \lambda_3^2 - 3, \tag{2}$$

where $\lambda_1, \lambda_2, \lambda_3$ are the principal stretch ratios (the ratios of stretched to unstretched lengths). The second relation for W, termed the Mooney–Rivlin form, is

$$W = C_1 J_1 + C_2 J_2, \tag{3}$$

where C_1 and C_2 are elastic coefficients with a sum $2(C_1 + C_2)$ equal to the shear modulus G and J_2 is a second symmetric measure of strain, independent of J_1:

$$J_2 = \lambda_1^{-2} + \lambda_2^{-2} + \lambda_3^{-2} - 3. \tag{4}$$

On expanding Eq. (3) as a power series in the strains e_i where $e_i = \lambda_i - 1$, it is found to include all terms in e^2 and e^3. Thus the Mooney–Rivlin form of strain energy necessarily gives good agreement with experiment at small strains.

Molecular theory of rubber elasticity suggests that the coefficient C_1 is proportional to the number N of molecular strands in the network per unit volume [3]. The coefficient C_2 appears to reflect additional physical restraints on molecular strands like those represented in the "tube" model [4], restraints that diminish in importance as the deformation increases. Because of this feature, Eq. (3) with constant C_2 gives poor agreement with measurements on rubber at quite modest strains, larger than about 10% [5]. Good agreement is obtained over a wide range of strains when the second term is replaced by a simple logarithmic function of J_2 [6]:

$$W = C_1 J_1 + C_2' \,\mathrm{Ln}[(J_2 + 3)/3]. \tag{5}$$

Values of C_1 and C_2' are found to be of similar magnitude, 0.25–0.5 MPa, for typical soft rubber vulcanizates.

2.2. Strain hardening at large strains

Rubber shows strain-hardening at large strains, probably because the long flexible molecular strands that comprise the material cannot be stretched indefinitely. The strain energy functions considered above do not possess this feature and therefore fail to describe stress–strain behavior at large strains. A strain-hardening feature can be introduced by a simple, although empirical, modification to the first term in Eq. (5), incorporating a maximum possible value for the strain measure J_1, denoted J_m, corresponding to a maximum possible stretch ratio for network strands [7]

$$W = -C_1 J_m \,\mathrm{Ln}(1 - J_1/J_m) + C_2' \,\mathrm{Ln}[(J_2 + 3)/3]. \tag{6}$$

An equivalent modification was proposed by Warner to provide strain-hardening for the bead–spring model of polymer molecules in a flowing solution [8]. Similarly, a limit can be imposed on possible values of J_2 by introducing a corresponding factor J_{2m} in the second term of Eq. (6) [9]. It should be noted, however, that $J_{1m}(=J_m)$ and J_{2m} cannot both be material constants because the relative values of J_1 and J_2 differ for different types of strain. As J_m represents the maximum stretch ratio for a typical network strand it is assumed to be a characteristic of the material, rather than J_{2m}.

Eq. (6) reduces to Eq. (3) when the strains are small and the ratio J_1/J_m is small and is thus probably the simplest strain energy function that accounts for the elastic behavior to good approximation over the whole range of strains. It requires three fitting parameters, two of which are related to the small-strain shear modulus G:

$$C_1 + C_2' = G/2. \tag{7}$$

The third parameter, J_m, is expected to be approximately proportional to Λ^2, where Λ is the maximum stretch ratio of an average strand in a network of long flexible strands. Moreover, Λ^2 is inversely proportional to N for strands that are randomly arranged in the unstretched state [3]. Thus, J_m is expected to be inversely proportional to C_1. The second coefficient, C_2', is found to be rather independent of the length and number of molecular strands comprising the network but decreases as the rubber is swollen by a compatible liquid, becoming negligibly small at a volume

swelling ratio of about 5. Thus, it appears to reflect physical restraints on molecular strands like those represented in the "tube" model, but the actual value is not yet predictable [4].

2.3. Stress–strain relations

Cauchy stresses t_i can be obtained from the relation for W by considering a hypothetical small change $d\lambda_1$ in the representative extension ratio λ_1 with force f_1. Since $\Delta W = f_1\, d\lambda_1$, the stress t_1 is given by

$$t_1 = \lambda_1 \partial W/\partial\lambda_1 + \Pi, \text{ etc.}, \tag{8}$$

where Π is an unknown hydrostatic pressure whose value is obtained in each case from the boundary conditions. Rewriting equations in terms of the generic derivatives $\partial W/\partial J_1$ and $\partial W/\partial J_2$ yields

$$t_1 = 2[\lambda_1^2 \partial W/\partial J_1 - (1/\lambda_1^2)\partial W/\partial J_2] + \Pi, \text{ etc.} \tag{9}$$

The functions $\partial W/\partial J_1$ and $\partial W/\partial J_2$ are denoted W_1 and W_2 hereafter.

For the strain energy function given in Eq. (6)

$$W_1 = C_1/[(1 - (J_1/J_m))] \tag{10}$$

and

$$W_2 = C_2'/(J_2 + 3). \tag{11}$$

When J_1 is small compared to J_m, W_1 is a constant (C_1), and at moderate strains the value of J_2 is often large enough for terms involving W_2 to be neglected. Some stress–strain relations are derived in the following sections using these approximations, at least initially, in order to deduce under what conditions the deformations become unstable.

3. Unstable deformations

3.1. Inflation of cylindrical tubes [10]

We consider here long thin-walled tubes, although the treatment is readily extended to deal with thick-walled tubes. For simplicity the constitutive law given in Eq. (6) is employed, with C_2' put equal to zero, i.e., with only two material parameters: C_1 and J_m.

The deformation is described by extension ratios λ_1 in the circumferential direction and λ_2 in the axial direction, with the wall thickness w becoming $w/\lambda_1\lambda_2$ because the rubber volume remains constant. For closed-end tubes, unconstrained in length, the inflation pressure P gives rise to stresses in the circumferential and axial directions

$$t_1 = \lambda_1^2\lambda_2 rP/w; \quad t_2 = \lambda_1^2\lambda_2 rP/2w, \tag{12}$$

where r is the tube radius in the unstrained state.

From Eq. (9), on putting the stress $t_3 = 0$, the undefined pressure Π is obtained as

$$\Pi = -2W_1/\lambda_1^2\lambda_2^2. \tag{13}$$

(In a thin-walled tube of large radius the inflating pressure P is much smaller than the stresses t_1 and t_2 that it generates and thus P can be neglected in comparison with the stress t_3 in determining Π.) Inserting this result for Π in Eqs. (9) and (12) yields a relation between the extension ratio λ_2 and the ratio v of the internal volume of the tube in the deformed state to that in the undeformed state

$$\lambda_2^3 = (v^2 + 1)/2v, \tag{14}$$

where $v = \lambda_1^2\lambda_2$. The relation between inflating pressure P and internal volume is then obtained as

$$Pr/wC_1 = 2(v^2 - 1)[2v/(v^2 + 1)]^{1/3}/v^2 \times[1 - (J_1/J_m)], \tag{15}$$

where J_1 is a function of the extension ratios, see Eq. (2), and hence also of v. Eq. (15) is plotted in Fig. 1 for various values of the limiting strain measure J_m. The inflating pressure is seen to pass through a maximum at a volume expansion ratio between about 58% and 66%, depending on the value assumed for J_m. This feature suggests that larger expansions will be unstable. Indeed, thin-walled tubes undergo a strikingly non-uniform deformation at a critical inflation pressure, shown schematically in Fig. 2. One portion of the tube becomes highly distended as a bubble or aneurysm while the rest remains lightly inflated. [1] Eq. (15) shows that in general two stable deformations can co-exist at the same inflation pressure after the critical state is reached, as shown schematically by the

[1] Professor Mahadevan of Cambridge University kindly drew my attention to the early work of Mallock [11] on unstable inflation of rubber tubes and balloons. Mallock predicted non-linear behavior and eventual instability on the basis of changes in the radius of shells under large inflations, retaining linear elastic behavior for the rubber. Thus, although he recognized that the basic phenomenon was due to elastic instability, his numerical conclusions differ appreciably from those reached here.

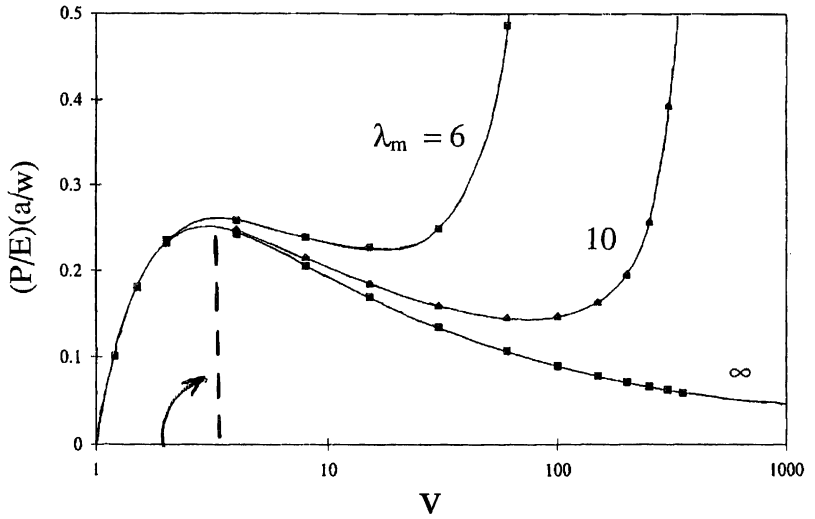

Fig. 1. Relation between inflation pressure P and volume expansion ratio v for a thin-walled tube, from Eq. (15). λ_m denotes the maximum possible extension ratio in simple extension [10].

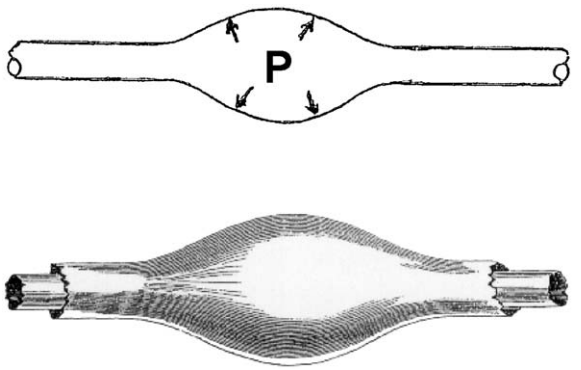

Fig. 2. Aneurysm in a tube inflated past the critical pressure and corresponding drawing by Mallock [11].

horizontal broken line in Fig. 1. However, when J_m is infinitely large the aneurysm is unbounded and failure would then occur immediately on reaching the critical pressure.

3.2. Inflation of a thin-walled spherical balloon [10]

In this case the deformation consists of an expansion of the balloon radius by a factor λ, causing equibiaxial extensions of ratio λ to be set up in the balloon and a shrinkage ratio $1/\lambda^2$ to occur in the wall thickness, to maintain the rubber volume constant. The circumferential stresses t_1 and t_2 created by the inflation pressure P are equal and given by

$$t = t_1 = t_2 = 2C_1(\lambda^2 - \lambda^{-4})/[1 - (J_1/J_m)] \qquad (16)$$

from Eq. (9), on putting the stress $t_3 = 0$.

The stresses set up in the balloon are generated by the inflation pressure P from Laplace's relation

$$Pr/w = 2t/\lambda^3, \qquad (17)$$

where r and w are the unstrained radius and wall thickness of the balloon.

The final result for the inflation pressure P as a function of the radial expansion ratio λ of the rubber shell is

$$Pr/wC_1 = 4(\lambda^{-1} - \lambda^{-7})/[1 - (J_1/J_m)]. \qquad (18)$$

Predictions of Eq. (18) are shown in Fig. 3 for three values of J_m corresponding to values of λ_m, the maximum possible extension ratio in simple extension, of 6, 10 and ∞. Again, they suggest that an instability will occur, in this case at a radial expansion ratio between 38% and 50%.

In practice, after a small initial inflation the deformation is quite complex. The balloon remains roughly

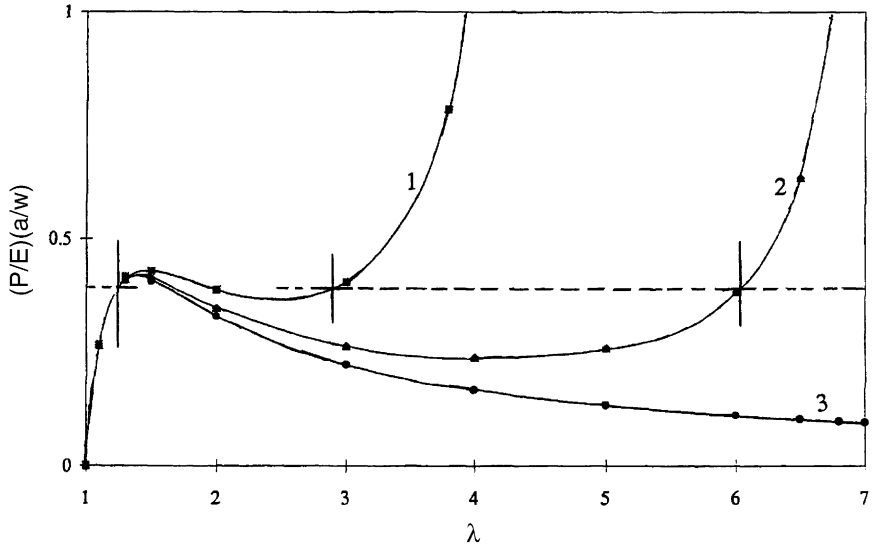

Fig. 3. Relation between inflation pressure P and radial expansion ratio λ for a balloon, from Eq. (18). Curves 1, 2 and 3 are for maximum possible extension ratios in simple extension of 6, 10 and ∞ [10].

spherical in shape but one part of it is lightly stretched while the remainder becomes highly stretched. The two states of strain resemble the two deformations that are predicted at a given pressure after the critical point is reached, as indicated schematically by the horizontal broken line in Fig. 3.

3.3. Inflation of a thick-walled spherical shell

The internal pressure P required to inflate a small spherical cavity in the center of a thick block can be obtained by integrating the contributions dP from concentric shells (thin-walled balloons) with a wall thickness dr. From Eq. (18)

$$r\,\mathrm{d}P = 4C_1(\lambda_r^{-1} - \lambda_r^{-7})/[1 - (J_1/J_m)]\,\mathrm{d}r, \qquad (19)$$

where λ_r is the stretch ratio at a radial distance r, and $J_1 = 2\lambda_r^2 + \lambda_r^{-4} - 3$. We note that the wall thickness $\mathrm{d}r/\lambda_r^2$ of a shell element in the strained state is equal to the increment $\mathrm{d}(\lambda_r r)$ in the strained radius. Thus

$$\mathrm{d}r/\lambda_r^2 = \mathrm{d}(\lambda_r r) = \lambda_r\,\mathrm{d}r + r\,\mathrm{d}\lambda_r. \qquad (20)$$

Eq. (19) becomes a differential equation for P in terms of the expansion ratio λ_r,

$$\mathrm{d}P/\mathrm{d}\lambda_r = -4C_1(\lambda_r^{-2} + \lambda_r^{-5})/[1 - (J_1/J_m)]. \qquad (21)$$

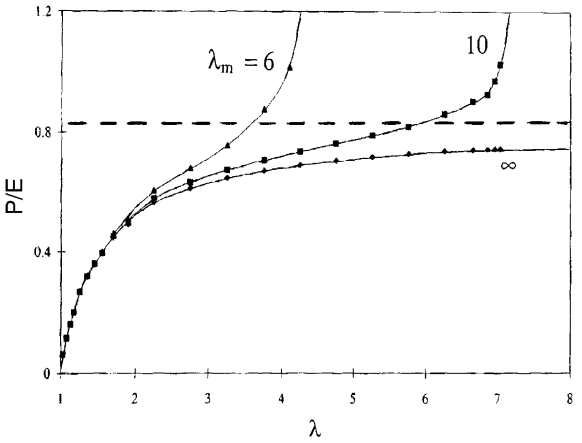

Fig. 4. Relation between inflation pressure P and expansion ratio λ of a spherical cavity in an infinitely large block, from Eq. (21) [10].

When Eq. (21) is integrated numerically, subject to the boundary condition that $P = 0$ at the far distant outer surface, where $r = \infty$ and $\lambda_r = 1$, the results shown in Fig. 4 are obtained. (The initial cavity radius r_o is denoted a in the figure.) When the inflation pressure P is plotted as a function of the expansion ratio λ of the cavity the curves do not generally exhibit a maximum and thus they do not show an obvious

instability. Instead, for highly extensible materials with large values of J_m, the pressure approaches a constant value of about $5C_1$ over a wide range of strains before rising sharply as the strain measure J_1 approaches J_m. However, when a contribution to the inflating pressure from the J_2 term is included in Eq. (21), then the pressure passes through a shallow maximum before rising again. Including the J_2 term, $[J_2 = \lambda_r^4 + 2/\lambda_r^2 - 3]$, Eq. (21) becomes

$$dP/d\lambda_r = -4C_1(\lambda_r^{-2} + \lambda_r^{-5})[1 - (J_1/J_m)] - 4C_2'(1 + \lambda_r^3)/\lambda_r(2 + \lambda_r^6). \quad (22)$$

The preceding results suggest that any small cavity will expand greatly at an inflation pressure of the order of $5C_1$, i.e., about $5E/6$, where E is the small-strain tensile modulus, and thus internal fracture is likely to occur in soft rubbery solids at inflation pressures of this amount. In practice, all rubbery solids are found to develop internal fractures when supersaturated with gases or liquids at pressures about equal to E, Figs. 5–7, or equivalently, subjected to hydrostatic tensions of this order, Fig. 8 [12,13]. The cavitation pressure for a dissolved gas is seen in Fig. 7 to be about equal to E for a number of rubbery solids.

Note that the initial radius of the spherical cavity does not appear in the equation for inflation pressure as a function of extension ratio λ of the cavity. Thus, cavities of all sizes are predicted to inflate by the same amount. However, surface energy effects will tend to stabilize small cavities and larger pressures will be required to inflate them [14]. Using typical values for the surface energy of hydrocarbon liquids, it appears that only cavities having radii greater than about 100 nm will expand dramatically at the relatively low pressures predicted here from purely elastic considerations. The experimental observations suggest that vulcanized rubber contains many precursor cavities of this effective size, or larger.

3.4. Surface instability of compressed or bent blocks

By considering the stability of surface deformational waves of various wavelength on a half-space of an incompressible neo-Hookean elastic material, Biot [15] showed that the surface will become unstable at a critical state of surface compression. Denoting the two axes parallel to the surface as 1 and 3, and the perpendicular axis as 2, Biot's result for the critical compressive stress t_1 in the 1-direction is

$$[1 - (\lambda_2/\lambda_1)]t_1 = \lambda_1(\partial t_1/\partial\lambda_1), \quad (23)$$

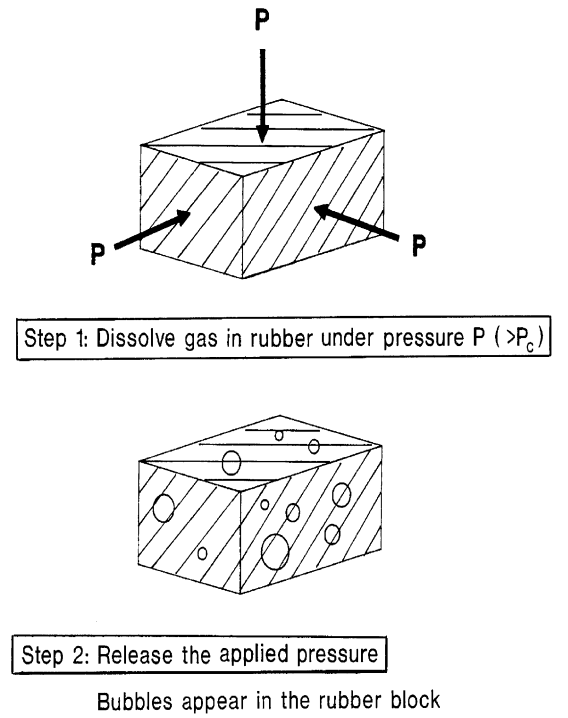

Fig. 5. Internal bubbles formed by dissolving a gas in rubber at a pressure P greater than a critical value P_c, and then releasing the applied pressure.

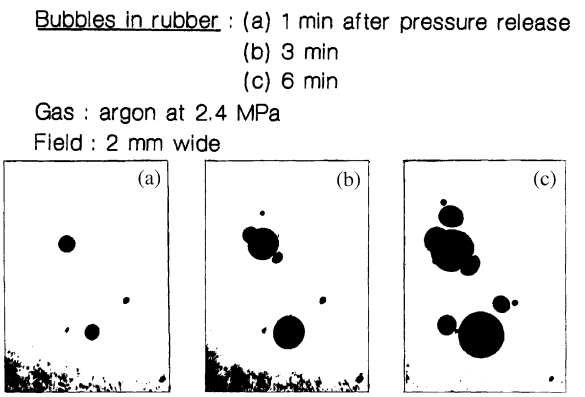

Fig. 6. Gas bubbles within a transparent rubber block supersaturated with argon gas. (a) 1 min after release of the external pressure (2.4 MPa); (b) 3 min; (c) 6 min. Field of view: 2 mm wide [13].

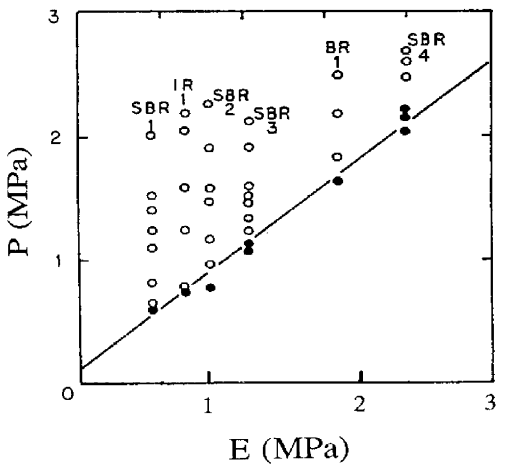

Fig. 7. Formation of internal bubbles by a dissolved gas at pressure P (open circles) vs. elastic modulus E of rubber. Filled circles: no bubbles formed. The line between filled and unfilled circles has a slope of $\frac{5}{6}$ [13].

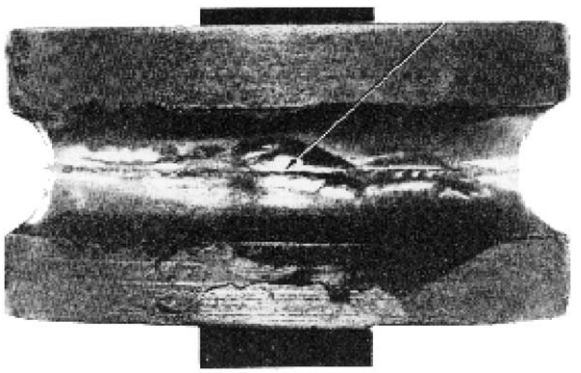

Fig. 8. Cavity formed in a bonded rubber block under a tri-axial tension in the center of about 2 MPa [12].

where $\partial t_1/\partial\lambda_1$ is the incremental (tangent) modulus in the strained state and $\lambda_1, \lambda_2, \lambda_3$, are the principal strain ratios. (Note that t_1 is the true (Cauchy) stress and λ_1, λ_3 are the strain ratios in the surface plane.)
From Eq. (9), the general stress–strain relation for an incompressible neo-Hookean material is

$$t_1 - t_2 = G(\lambda_1^2 - \lambda_2^2), \tag{24}$$

where G is the shear modulus. In the present case the stress t_2 applied normal to the surface is zero and $\lambda_2 = 1/\lambda_1\lambda_3$. On substituting for t_1 and $\partial t_1/\partial\lambda_1$ from Eq. (9), Eq. (23) becomes a relation between the critical strain ratios λ_1, λ_3 in the directions parallel to the surface at which the surface becomes unstable. It can be reformulated as

$$z^3 + z^2 + 3z - 1 = 0, \tag{25}$$

where $z = \lambda_1^2\lambda_3$. The solution of Eq. (25) is

$$z(=\lambda_1^2\lambda_3) = 0.2956. \tag{26}$$

Surface instabilities in compressed rubber blocks have also been analyzed by Usmani and Beatty [16] and Best et al. [17]. Their results agree with those obtained by Biot.

Some special cases are now considered. First, when the block is subjected to simple unidirectional compression parallel to the surface, with free expansion permitted in the other two directions, then $\lambda_3 = 1/\lambda_1^{1/2}$. Eq. (26) then yields a critical value for λ_1 of 0.444. Thus, a large block of rubber in simple compression is predicted to exhibit a surface instability at a compression of 55.5%. In an analysis of bending deformations, Levinson [18] and Fosdick and Shield [19] predicted that a bending instability would occur in a neo-Hookean block at this degree of compression. However, in a review of the stability of compressed rubber blocks, Beatty noted that various buckling and bulging modes of deformation are generally encountered before this, depending on the slenderness of the block [20].

When expansion is prevented in the three-direction parallel to the surface ($\lambda_3 = 1$), so that the block undergoes plane-strain compression, then the critical value for λ_1 predicted by Eq. (26) is 0.544. And if the block is subjected to equi-biaxial compression parallel to the surface, $\lambda_3 = \lambda_1$, the critical strain ratio becomes 0.666. The latter case is considered further in Section 3.6.

Note that all of these critical strains correspond to relatively small values of the strain invariant J_1, of about 1.70, 1.68 and 2.97, respectively. These values are much smaller than the maximum values J_m attainable in normal rubbery materials, which lie in the range 20–200. It is therefore not generally necessary to incorporate finite-extensibility effects when considering the stability of compressed blocks.

When a thick elastic block (cuboid) is bent, the inner surface becomes compressed. The extension ratio λ_3 along the width would be expected to remain unchanged at unity (plane strain) because tensile stresses

in the outer layers are more-or-less balanced by compressive stresses in the inner layers. Thus, an instability would be expected on the inner surface from Biot's analysis, when λ_1 is 0.544, i.e., when the surface compression there is about 46%.

Experimentally, sharp folds or creases appear suddenly in the inner surface of a bent block, at a critical degree of bending [21]. Typical creases are shown in Fig. 9. Surface strains were determined when the creases first appeared, of 45% extension on the outer surface and 35% compression on the inner surface, reasonably consistent with calculated values for surface strains in a bent cuboid. And, as expected, the width did not change appreciably on bending. However, the critical strains were considerably smaller than predicted by Biot's theory, 83% extension on the outer surface and 46% compression on the inner surface.

It is not clear why the instability occurred so much sooner than expected. Although rubber is known to follow a more complex strain energy function than the neo-Hookean form, it seems unlikely that the difference, particularly at relatively moderate compressive strains, would have such marked consequences.

3.5. Implications of surface instability in compression

Rubber articles are often subjected to rather severe bending deformations, for example, in tires. The inner (compressed) surface is largely concealed and folds and creases may pass undetected. Nevertheless, they represent lines of high stress concentration and sites of possible premature failure. Folds ("Schallamach waves") also appear in rubber surfaces under frictional forces. Motion of the folds is an important sliding mechanism for soft rubber [22], and it seems likely that they also play a role in rubber abrasion. Their formation was attributed to local buckling of the surface under compressive stresses in the surface plane. Best et al. [17] showed that they will appear at higher frictional forces in rubber stretched in the sliding direction and at lower frictional forces in rubber compressed in this direction, in accord with observation [23]. Further elucidation of the critical conditions under which surface folds and creases appear seems highly desirable.

3.6. Resistance of a compressed block to indentation

When a block is subjected to a sufficiently large equibiaxial compression in the plane parallel to the surface, it becomes unstable to small surface indentations. Green and Zerna [24] expressed the relation between indentation force N and amount of indentation d as

$$N/G = (8/3)R^{1/2}d^{3/2}f(\lambda), \tag{27}$$

where G is the shear modulus of the half-space material, R is the radius of the indentor and $f(\lambda)$ is a function of the equibiaxial compression ratio λ, given by

$$f(\lambda) = (\lambda^9 + \lambda^6 + 3\lambda^3 - 1)/\lambda^4(\lambda^3 + 1). \tag{28}$$

When the half-space is not compressed initially, i.e., $\lambda = 1$, Eq. (27) reduces to the well-known Hertz form

$$N/G = (16/3)R^{1/2}d^{3/2}. \tag{29}$$

Values of indentation force N for a given small indentation, from Eq. (27), are plotted in Fig. 10 against the equibiaxial strain e parallel to the surface, where $e = \lambda - 1$. (N_0 denotes the value for an initially-unstrained block, given by Eq. (29).)

The resistance to indentation is seen to decrease sharply as the compressive strain is increased, becoming zero at a compressive strain of 0.333, in agreement with Biot's result given in the preceding section: $\lambda = 0.666$. On the other hand, moderate extensions seem to have little effect on the resistance to indentation.

3.7. Torsional instability of stretched rubber rods [25]

When a stretched rubber rod is subjected to large torsions, a kink suddenly appears at one point along the rod, Fig. 11. More kinks form on twisting the rod further. Considerations of the stability of a stretched rubber rod, outlined below, suggest that it will become unstable at a critical amount of torsion; part of the rod will unwind and form a tight ring or kink while the remainder of the rod becomes more stretched. A simple criterion can be derived on this basis for the onset of kinks. More complex deformations, buckling and writhing, have been considered by Thompson and Champneys [26,27].

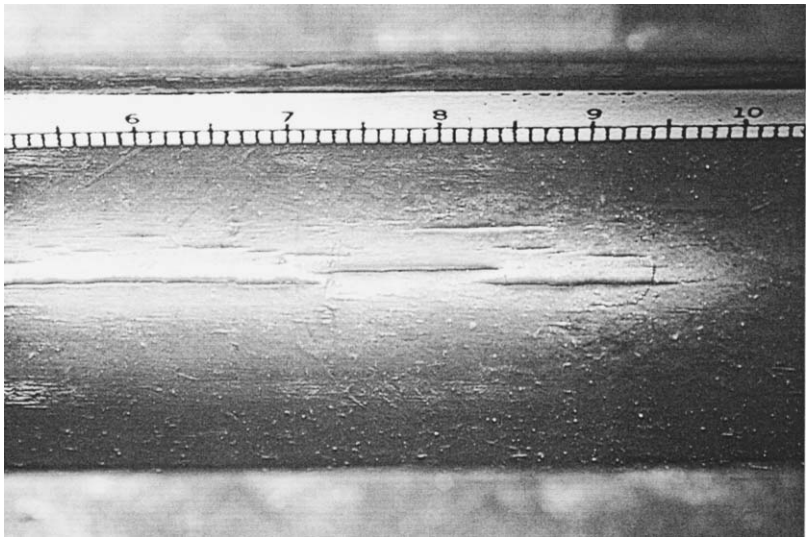

Fig. 9. Creases, 5–10 mm long, formed suddenly on the inner surface of a bent block at a critical compressive strain [21].

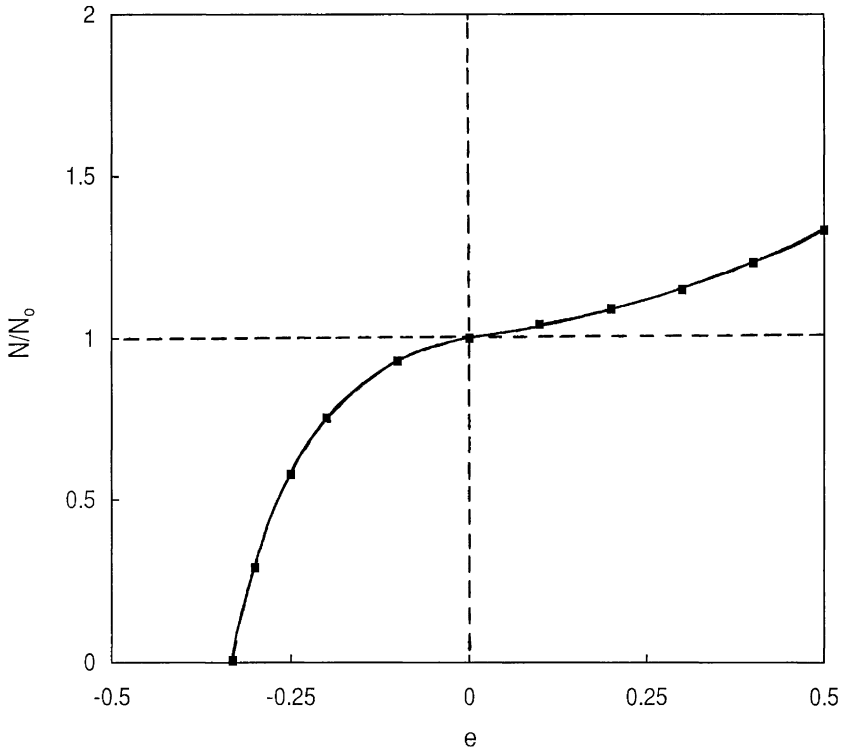

Fig. 10. Force N for a given indentation by a spherical indentor vs. equibiaxial strain e in the surface of a half-space (N_o is the force when $e = 0$).

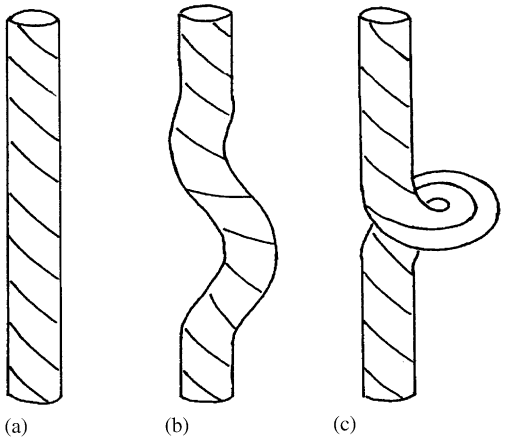

Fig. 11. (a–c) Kink formation on twisting a stretched rubber rod.

We consider for simplicity a long rod of a neo-Hookean material with initial length L_o and radius a, stretched to an extension ratio λ and twisted by an angle ϕ per unit of stretched length. The stresses set up have been calculated by Rivlin [1,2]. From Eq. (1), energy dW is stored in a cylindrical tubular element of radius r, thickness dr and stretched length L:

$$dW = GJ_1 \pi L r \, dr, \tag{30}$$

where $L = \lambda L_o$ and $J_1 = \lambda^2 + 2/\lambda + \lambda^2\phi^2 r^2 - 3$ [28]. On integrating between $r = 0$ and $a/\lambda^{1/2}$, the total strain energy W is obtained as

$$W = \pi a^2 L_o C_1 [\lambda^2 + 2/\lambda - 3 + \lambda a^2 \phi^2/2]. \tag{31}$$

If part of the twisted rod is transformed into a horizontal ring, the number N of complete turns in the twisted rod is reduced to $N-1$ and the length of the remainder of the rod is increased by the difference between the length (thickness) of a horizontal ring, $2a/\lambda^{1/2}$, and the length of the same portion of the rod in its original state, i.e., L/N. [Note that $L/N = 2\pi/\phi$.] The extension ratio is therefore increased by an amount

$$d\lambda = (2\pi/\phi - 2a/\lambda^{1/2})/L_o. \tag{32}$$

Thus, due to the net effect of an increase in extension ratio and a decrease in torsion, the strain energy W of the twisted portion of the rod is increased by an amount ΔW:

$$\Delta W/\pi a^2 C_1 = 4[(\lambda - 1/\lambda^2) + (a^2\phi^2/4)] \times (\pi/\phi - a/\lambda^{1/2}) - 2\pi a^2 \phi. \tag{33}$$

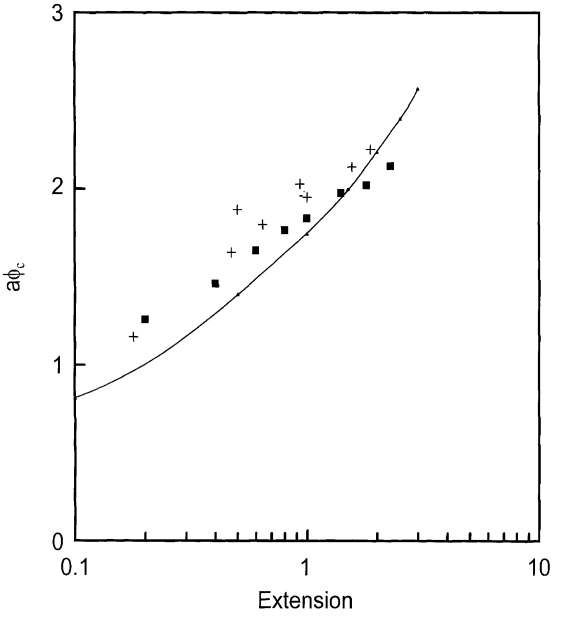

Fig. 12. Critical amount of torsion $a\phi_c$ (rad) vs. tensile strain e. Rod radius $a = 2.45$ mm (squares); 7.35 mm (crosses). Curve calculated from neo-Hookean theory, Eq. (34).

ΔW becomes zero when

$$4(1 - 1/\lambda^3) = -(a^2\phi^2/\lambda) + 2\pi(a^2\phi^2/\lambda)/ \times [\pi - (a\phi/\lambda^{1/2})]. \tag{34}$$

Eq. (34) gives critical values $a\phi_c$ for the amount of torsion at which uniform torsion becomes unstable, in terms of the imposed extension ratio λ. The results are plotted as a continuous curve of $a\phi_c$ vs. λ in Fig. 12. Some experimental measurements of the critical amount of torsion at which a kink suddenly appeared in rubber rods of various diameters, stretched to various extents, are plotted as points in Fig. 12. They are seen to be in reasonably good agreement with the theoretical predictions, indicating that the sudden formation of kinks in twisted rubber rods is, indeed, a consequence of an elastic instability.

4. Concluding remarks

Several novel elastic instabilities of rubbery materials have been described and accounted for in terms of the theory of large elastic deformations. No doubt

others remain to be discovered. Instabilities are interesting from a theoretical point of view because they occur suddenly, at a well-defined deformation. A comparison of the observed onset of instability with the predictions of various strain energy functions W thus provides, at least in principle, a critical test for the validity of a proposed form for W. From a practical standpoint, unstable states are quite undesirable and should be avoided because the deformation becomes highly non-uniform, leading to premature failure.

References

[1] R.S. Rivlin, Philos. Trans. Roy. Soc. Lond. Ser. A 241 (1948) 379–397.
[2] R.S. Rivlin, in: F.R. Eirich (Ed.), Rheology, Theory and Application, Vol. 1, Academic Press, New York, 1956 (Chapter 10).
[3] L.R.G. Treloar, The Physics of Rubberlike Elasticity, 3rd Edition, Clarendon Press, Oxford, 1975.
[4] W.W. Graessley, Polymeric Liquids and Networks: Structure and Properties, Garland Science, New York, 2004 (Chapter 10).
[5] R.S. Rivlin, D.W. Saunders, Philos. Trans. Roy. Soc. Lond. Ser. A 243 (1951) 251–288.
[6] A.N. Gent, A.G. Thomas, J. Polym. Sci. 28 (1958) 625–628.
[7] A.N. Gent, Rubber Chem. Technol. 69 (1996) 59–61.
[8] H.R. Warner Jr., Ind. Eng. Chem. Fund. 11 (1972) 379–387.
[9] E. Pucci, G. Saccomandi, Rubber Chem. Technol. 75 (2002) 839–851.
[10] A.N. Gent, Rubber Chem. Technol. 72 (1999) 263–268.
[11] A. Mallock, Proc. Roy. Soc. Lond. 49 (1890–1891) 458–463.
[12] A.N. Gent, P.B. Lindley, Proc. Roy. Soc. Lond. A 249 (1958) 195–205.
[13] A.N. Gent, D.A. Tompkins, J. Appl. Phys. 40 (1969) 2520–2525.
[14] A.N. Gent, D.A. Tompkins, J. Polym. Sci. Part A-2 7 (1969) 1483–1488.
[15] M. Biot, Appl. Sci. Res. Sec. A 12 (1963) 168–182; M. Biot, Mechanics of Incremental Deformations, Wiley, New York, 1965.
[16] S.A. Usmani, M.F. Beatty, J. Elasticity 4 (1974) 249.
[17] B. Best, P. Meijers, A.R. Savkoor, Wear 65 (1981) 385.
[18] R.L. Fosdick, R.T. Shield, Arch. Ration. Mech. Anal. 12 (1963) 223.
[19] M. Levinson, J. Mech. Phys. Solids 16 (1968) 403.
[20] M.F. Beatty, in: R.S. Rivlin (Ed.), Finite Elasticity, AMD, Vol. 27, American Society of Mechanical Engineers, New York, 1977, p. 125.
[21] A.N. Gent, I.S. Cho, Rubber Chem. Technol. 72 (1999) 253–262.
[22] A. Schallamach, Wear 17 (1971) 301.
[23] M. Barquins, R. Courtel, D. Maugis, Wear 38 (1976) 385.
[24] A.E. Green, W. Zerna, Theoretical Elasticity, 2nd. Edition, Clarendon Press, Oxford, 1975, Section 4.6, p. 135.
[25] A.N. Gent, K.-C. Hua, Int. J. Non-Linear Mech. 39 (2004) 483–489.
[26] J.M.T. Thompson, A.R. Champneys, Proc. Roy. Soc. Lond. A 452 (1996) 117–138.
[27] A.R. Champneys, J.M.T. Thompson, Proc. Roy. Soc. Lond. A 452 (1996) 2467–2491.
[28] M.F. Beatty, Appl. Mech. Rev. 40 (1987) 1699–1734.